

**Title**

**Holocene phreatomagmatic eruptions alongside the densely populated northern shoreline of Lake Kivu, East-African Rift: timing and hazard implications**

**Authors**

Sam Poppe<sup>1</sup>, Benoît Smets<sup>1,2,3</sup>, Karen Fontijn<sup>4</sup>, Montfort Bagalwa Rukeza<sup>5</sup>, Antoine De Marie Fikiri Migabo<sup>5</sup>, Albert Kyambikwa Milungu<sup>5</sup>, Didier Birimwiragi Namogo<sup>5</sup>, François Kervyn<sup>3</sup>, Matthieu Kervyn<sup>1</sup>

**Author affiliations**

1) Department of Geography, Earth System Science, Vrije Universiteit Brussel, Pleinlaan 2, B-1050 Brussels, Belgium

2) European Center for Geodynamics & Seismology, 19 Rue Josy Welter, 7256 Walferdange, Grand Duchy of Luxembourg

3) Department of Earth Sciences, Royal Museum for Central Africa, 13 Leuvensesteenweg, 3080 Tervuren, Belgium

4) Department of Earth Sciences, University of Oxford, South Parks Road, Oxford OX1 3AN, United Kingdom

5) Goma Volcano Observatory, 142 Avenue Rond-Point, Goma, Democratic Republic of the Congo

**Corresponding Author**

Sam Poppe: sam.poppe@vub.ac.be

Tel.: +32-2-629 35 56

**Keywords**

Virunga Volcanic Province, Lake Kivu, phreatomagmatism, dilute pyroclastic density current, volcanic hazard

## **ABSTRACT**

The Virunga Volcanic Province (VVP) represents the most active zone of volcanism in the western branch of the East African Rift System. While the VVP's two historically active volcanoes, Nyamulagira and Nyiragongo, have built scoria cones and lava flows in the adjacent lava fields, several small phreatomagmatic eruptive centers lie along Lake Kivu's northern shoreline, highlighting the potential for explosive magma-water interaction. Their presence in the densely urbanized Sake-Goma-Gisenyi area necessitates an assessment of their eruptive mechanisms and chronology. Some of these eruptive centers possess multiple vents, and depositional contacts suggest distinct eruptive phases within a single structure. Depositional facies range from polymict tuff breccia to tuff and loose lapilli, often impacted by blocks and volcanic bombs. Along with the presence of dilute pyroclastic density current (PDC) deposits, indicators of magma-water interaction include the presence of fine palagonitized ash, ash aggregates, cross-bedding and ballistic impact sags. We estimate that at least 15 phreatomagmatic eruptions occurred in the Holocene, during which Lake Kivu rose to its current water level. Radiocarbon dates of five paleosols in the top of volcanic tuff deposits range between ~2,500 and ~150 cal. yr BP, and suggest centennial- to millennial-scale recurrence of phreatomagmatic activity. A vast part of the currently urbanized zone on the northern shoreline of Lake Kivu was most likely impacted by products from phreatomagmatic activity, including PDC events, during the Late Holocene, highlighting the need to consider explosive magma-water interaction as a potential scenario in future risk assessments.

## **INTRODUCTION**

Although the Virunga Volcanic Province (VVP) is mostly known for its effusive volcanism, the presence of phreatomagmatic centers with a young morphology along Lake Kivu's densely populated northern shoreline signals the need to consider the future hazard of

explosive magma-water interactions. The VVP lies at a transfer zone that separates two rift segments (i.e. Kivu and Albert rifts; Ebinger 1989; Smets et al. 2016) within the western branch of the East African Rift (Fig. 1a-b). The VVP hosts eight large volcanic edifices, of which Nyiragongo and Nyamulagira, in the western, intra-rift part of the VVP, have frequently erupted over the past 150 years. Nyamulagira is a flow-dominated shield volcano (e.g. Smets et al. 2015). Nyiragongo is a stratovolcano complex with a semi-permanent lava lake (Fig. 1; e.g. Tazieff 1977, Komorowski et al. 2003). Both edifices' flanks and their adjacent lava fields are occupied by >200 satellite eruptive centers, most of which are scoria cones. The southernmost centers along the northern shoreline of Lake Kivu stand out due to their poorly documented phreatomagmatic nature (Fig. 1).

Denaeyer (1975) provided morphological and preliminary stratigraphic descriptions of the satellite center deposits along Lake Kivu's northern shoreline, and Tuttle et al. (1990) suggested these deposits represent a potential explosive eruptive hazard in the area, based on stratigraphic facies and two radiocarbon dates ( $740 \pm 110$  yr BP and  $10,240 \pm 30$  yr BP; Table 1). Capaccioni et al. (2003) present a geochemical study of some of the small eruptive centers and suggest a petrogenetic relationship between the magma which fed these centers and the highly alkaline, silica-undersaturated magmas which feed Nyiragongo's main edifice. These studies recognize the phreatomagmatic nature of most eruptive centers within a 2 km distance of the lake shore, in contrast to the dry magmatic nature of the centers further up the main edifices' flanks. The presence of >1.2 million inhabitants in the Sake-Goma-Gisenyi urban area (Fig. 1c) necessitates a detailed hazard assessment based on stratigraphic descriptions and absolute chronology of the phreatomagmatic deposits.

In this study, we identify evidence of explosive magma-water interaction in key lithofacies of the small eruptive centers along the northern shoreline of Lake Kivu. We further propose more detailed eruptive scenarios for the two best exposed complexes, Mt Goma and Lac Vert

(Fig. 1), and provide a radiocarbon chronology of phreatomagmatic eruptions in the area, put into the context of Holocene lake level variations of Lake Kivu. Finally, we discuss the implications for this phreatomagmatic hazard in the densely populated Sake-Goma-Gisenyi urban area.

## **PHREATOMAGMATISM: CONCEPTS AND DEFINITIONS**

The term ‘phreatomagmatism’ defines eruptions in which magma interacts explosively with external water (Houghton et al. 2015). External water is vaporized upon contact with ascending hot magma, which is in turn efficiently fragmentated into relatively fine-grained pyroclasts as compared to coarser fragments formed in dry magmatic eruptions during which fragmentation is driven purely by degassing of magmatic volatiles (e.g. Kokelaar 1986, Zimanowski et al. 1997). The explosivity of the magma-water interactions often results in the excavation of bedrock. Complex environmental controls at the eruptive vent can result in either simple evolution or complex back-and-forth shifting between contrasting phreatomagmatic and magmatic styles during an eruptive phase. Factors controlling the eruptive style include varying influx rates of external water, variations in magma ascent rate and patterns and rates of magma degassing (e.g. Kokelaar 1986, Wohletz 1986, Houghton et al. 1999, Németh et al. 2012).

Mafic magma quenched rapidly by external water forms sideromelane fragments which can be recognized in thin section by their yellow-brown translucence and isotropic character. Sideromelane is often altered to form the material “palagonite”, which comprises hydrated glass and smectitic clays, often associated with zeolites (e.g. Pauly et al. 2011). In the eruption plume, moist ash can aggregate into accretionary lapilli, which commonly have a concentric structure. Accretionary lapilli with a solid clast core are called armored lapilli (Fisher and Schmincke 1984).

During the 1963 Surtsey (White and Houghton 2000) and 1965 Taal (Moore et al. 1966), eruptions, small-scale phreatomagmatic eruptions occurred as a succession of intermittent explosions. The ratio of magma to water at the fragmentation locus in the vent largely controls the density and temperature of the erupted mixture of pyroclasts, magmatic gases and water vapor (Koyaguchi and Woods 1996). The pulsating phreatomagmatic plume formed from this mixture often becomes too dense to remain buoyant in air and instead generates ground-hugging dilute pyroclastic density currents (PDC), which expand laterally away from the vent (e.g. Schmincke et al. 1973, Brand and Clarke 2012, Van Eaton et al. 2012). These types of PDCs have historically been termed ‘base surges’, but the more general term ‘dilute PDC’ is preferred here (Manville et al. 2009, White and Ross 2011). The spatial extent and sedimentological features of PDC deposits, e.g. cross-bedding and dune wavelengths, help inferring the variations in the controlling factors which control PDC run-out distance (e.g. Valentine and Fischer 2000, Brand and Clarke 2012, Brand et al. 2014). Volcanic constructs dominantly formed by explosive magma-water interaction often display a wide range of magmatic and phreatomagmatic lithofacies. Based on their morphology they are subdivided into tuff cones, tuff rings and maars (Manville et al. 2009, Ross and White 2011).

## **METHODOLOGY**

Two field missions were undertaken in 2013, during which volcanic deposits associated with small eruptive centers within 2 km of the Lake Kivu shoreline were described for geometry, texture and lithological componentry. We adopt the nomenclature of volcanoclastic deposits as proposed by White and Houghton (2006). Accessibility of outcrops is typically best in populated areas where scoria and coarse ash are quarried as construction sands. Where deposits were inaccessible, we complement our observations with those of Denaeyer (1975)

and Capaccioni et al. (2003). Geographic coordinates of outcrop and sample locations are given in Supplementary Table S1. Qualitative observations of clast type and componentry of representative facies were performed on thin sections. We collected 12 paleosol samples and one gastropod shell from seven different horizons for radiocarbon dating of the most recent phreatomagmatic activity in the area (Table 1). Samples were preferentially collected from the soils in the uppermost parts of the deposits immediately below overlying, more recent lava flows. Analysis was performed at Beta Analytic Inc. (Florida, USA) using Accelerator Mass Spectrometry. The resulting ages were calibrated in OxCal v4.2 (<http://www.c14.arch.ox.ac.uk>; Bronk Ramsey 2009; Table 1), using the IntCal13 calibration curve (Reimer et al. 2013).

## **STRATIGRAPHY AND CHRONOLOGY OF PHREATOMAGMATIC COMPLEXES**

Depositional and clast characteristics of the studied deposits at the small eruptive centers define five contrasting lithofacies, interpreted as phreatomagmatic or magmatic in origin (Table 2; Fig. 2). Using these lithofacies, we describe the complex internal stratigraphy of the two best exposed complexes, Mt Goma and Lac Vert, as well as eruptive units at two additional cones.

### **The Mt Goma tuff cone complex**

Mt Goma (MGO) is located within the city center of Goma, at the shoreline of Lake Kivu (Fig. 1). It is a complex of three to four craters, the largest of which is breached into the lake and used as the city's harbor (Fig. 3). The Mt Goma magma has a silica-undersaturated foiditic bulk composition and is geochemically related to central Nyiragongo lavas (melilite or leucite-bearing nephelinites; Capaccioni et al. 2003). We distinguish three major eruptive units, based on facies characteristics and bedding dip directions (Figs. 3, 4):

151 Phase **MGO-P1** is exposed at the southern cliffs which are eroded by the lake waves (Fig. 4).  
152 The beds were sourced from the southernmost and smallest crater P1 (~175 m diameter) of  
153 the complex, as can be inferred from their crater-inward dip (Fig. 3). This first unit is  
154 maximum 25 m thick, divided in dm-scale beds of consolidated Facies 2 tuff and lapilli tuff  
155 (Fig. 2c-f, 4a). The fine ash matrix is dark brown and individual particles have a yellow  
156 palagonite rim, responsible for the ochre color of the deposits (Fig. 2e-f).

157 Phase **MGO-P2** is exposed at the summit rim and within the central subaerial crater. Crater-  
158 inward dips of the beds are consistent with this crater as their point of origin (Fig. 3). The  
159 crater has a diameter of 300 - 400 m and a maximum depth of 100 m. The MGO-P2 unit is  
160 minimum 10 m thick and comprises Facies 3a unconsolidated fine and coarse tuffs with cross-  
161 laminations (Figs. 2, 4b). MGO-P2 is separated from MGO-P1 to the South by a sudden  
162 upward decrease in consolidation.

163 **MGO-P3** is the most voluminous phase and forms the entire northern part of the eruptive  
164 complex. Subaerial morphology and bedding dips suggest that the vent of origin corresponds  
165 to the bay of Goma harbor (Fig. 3). Immediately NW of the MGO-P2 crater, MGO-P3 beds  
166 truncate the MGO-P2 tuffs. The MGO-P3 subunits are each 0.5-2 m thick and alternate  
167 between Facies 3a coarse-and-fine tuffs and Facies 3b tuff and lapilli tuff (Figs. 2g-j). The  
168 latter facies becomes more abundant upwards in the section, as the proportion of fine ash  
169 decreases (Figs. 4c-d). Deposits are generally (sub)parallel bedded, with m-scale undulations,  
170 pinch-and-swell and chute-and-pool structures and occasionally erosional channels. The entire  
171 sequence contains varying amounts of subangular cm- to m-sized, poorly vesicular lava  
172 blocks which contain 1 – 40 vol% nepheline and leucite crystals. These blocks are interpreted  
173 as accidental lithics disrupted from pre-MGO lava flows (Denaeyer 1975). The largest lithic  
174 blocks created impact sags in underlying beds in the lowermost subunits of MGO-P3, whereas  
175 lithic blocks and vesicular bombs perforated the bedding in the upper part.

A >3 km wide sublacustrine fan extends SW from Mt Goma to >250 m below the current lake level (Fig. 1c; Ross et al. 2014). This fan could represent either the subaqueous continuation of the complex, or a debris fan originating from a collapsed, subaerial part of Mt Goma. Quarried sections of Facies 3a tuffs of the outer flank sequence are exposed on land tens of meters away from the northern morphological base of the complex (Fig. 4e). In these quarries, the thickness of these tuffs is still >3 m. These tuffs are overlain by a ~1 m-thick lava flow, identified as the voluminous 'Buyinga' flow which covers a large part of Nyiragongo's southern flank on the map by Thonnard et al. (1965) (Fig. 4e). The extent of MGO-P3 deposits well beyond the Mt Goma cone suggests that the subaerial cone is the summit of a much larger eruptive complex which has its base >250 m below the current lake level (Fig. 1c).

Tuttle et al. (1990) obtained an age of  $703 \pm 97$  a cal. BP on a charcoal sample from within the top unit of the MGO-P3 tuffs (Lk-89-04; Table 1; Figs. 3, 5). Two newly collected samples from the poorly developed paleosol above MGO-P3 and directly below the overlying Buyinga lava flow (Fig. 4e), were dated at  $749 \pm 37$  a cal. BP (13MGO190201) and  $611 \pm 37$  a cal. BP (13MGO190202; Table 1; Fig. 5). These ages are consistent with the results of Tuttle et al. (1990) and suggest that the minimum eruptive age for the upper part of Mt Goma ranges between ca. 900 and 550 a. This age also represents the oldest possible eruptive age range of the Buyinga lava flow.

### **The Lac Vert maar volcano**

Lac Vert (LVE), i.e. Green Lake, is located west of Goma city and ~2 km north of the Lake Kivu shoreline (Fig. 1). Lac Vert volcanic rocks possess a Nyiragongo-like, silica-undersaturated foidite composition, but with lower alkali concentrations than those of Mt Goma (Chakrabarti et al. 2009). Lac Vert classifies as a maar complex, formed by three



201 craters and an adjacent tephra ring, with the floor of its largest lake-occupied crater lying  
202 below the surrounding topography (Fig. 6). The complex has a WSW-ENE elongated shape  
203 and scalloped rim, which is breached in the northern and southeastern parts. Three major  
204 eruptive phases were discriminated (Fig. 7):

205 Phase **LVE-P1** originated from the southern inundated crater, as suggested by the crater-  
206 outward bedding dip (Fig. 6), and consists of two subunits (Fig. 7). **LVE-P1-1** is exposed in  
207 the eastern crater cliff and is a Facies 1 polymict tuff breccia consisting of mm- to m-sized  
208 crystal-rich lithic blocks from pre-LVE lava flows with a minor amount of rounded and  
209 elongated pebbles, possibly sourced from an ancient river bed below the volcanic rocks (Figs.  
210 2a, 7a). The fine-grained matrix consists of ~50 vol% submillimetric vesicular lapilli and  
211 vitric juvenile ash, and ~50% subangular lithic clasts from pre-LVE lava flows and the  
212 crystalline basement. This non-bedded tuff breccia grades upward into the **LVE-P1-2** Facies 2  
213 consolidated, cross-bedded and palagonitized tuffs and lapilli tuffs with block impact sags and  
214 armored lapilli (Fig. 2d, 7b). The top portion of LVE-P1-2 is exposed in the easternmost  
215 quarries and its yellow-orange color is ascribed to pervasive alteration (Fig. 7c).

216 Phase **LVE-P2** was sourced from the northern crater with a diameter of 300-400 m as  
217 suggested by the surrounding bedding dip orientations (Fig. 6). The 2–15 m thick Facies 3a  
218 coarse and fine tuffs are found on top of LVE-P1 over the entire edifice (Figs. 2h, 7c-d). The  
219 rocks of this facies are quarried as construction sands. Vertical 10-30 cm displacements of the  
220 LVE-P2 beds along small normal faults occurred on the steep slopes of the LVE-P1 upper  
221 surface. We infer these displacements are syn-depositional since they terminate within  
222 portions of the sequence and never affect the entire sequence.

223 Phase **LVE-P3** is spatially limited to the 80 by 100 m wide crater nested within the larger  
224 northern crater (Fig. 6). LVE-P3 is a small-volume Facies 1 polymict tuff breccia and  
225 contains massive lava blocks of pre-LVE origin, incorporated in a crudely bedded fine grey

ash matrix, which consists of ~50 vol% juvenile vitric ash and ~50% lithic clasts from pre-LVE lava flows and the crystalline basement (Fig. 2b). Its discordant position against the intra-crater wall of LVE-P1-2 tuffs and the absence of LVE-P2 tephra in the LVE-P3 crater itself suggests that LVE-P3 represents the most recent eruptive phase of the Lac Vert complex.

Fossil shells found burrowed *in situ* in the weathered upper few cm of LVE-P1 at the easternmost outer flank were determined as the terrestrial gastropod *Limicolaria* sp. *Schumacher* (D. Van Damme pers. comm. 2014; Crowley and Pain 1970). One shell yielded a radiocarbon age of  $1,024 \pm 43$  a cal. BP (13LVE240202a; Table 1, Fig. 5), whereas the surrounding paleosol yielded  $2,124 \pm 78$  a cal. BP (13LVE240202b). At the same stratigraphic but intra-crater position below LVE-P2, a paleosol sample in the top of LVE-P1 yielded an age of  $2,334 \pm 37$  a cal. BP (13LVE1402). Both paleosol ages define a minimum LVE-P1 eruptive age range of ca. 2,380-2,000 a (Fig. 5), while the age of the *Limicolaria* shell constrains the maximum eruptive age range of the overlying LVE-P2 at ca. 1,175-950 a.

A small ~20 m long, ~30 m wide pahoehoe lava flow lobe invaded Lac Vert in its easternmost corner (Fig. 6), but field relations could not establish if it is part of the LVE complex, or of a more recent lava flow. The entire outer base of the LVE edifice is covered by 1-3 m thick lava flows. Two samples from the paleosol below a post-LVE lava flow in the eastern breach (Fig. 7d) yielded ages of  $378 \pm 48$  and  $382 \pm 47$  a cal. BP, respectively (13LVE1301 and 13LVE1201; Fig. 5). Two paleosol samples taken below a lava flow covering the NNE slopes yielded ages of  $608 \pm 35$  and  $638 \pm 40$  a cal. BP (13LVE1002a and 13LVE1002b, Fig. 5). These four samples most likely date two separate lava flows to expected age ranges of ca. 465-295 a and 685-555 a respectively. The latter age provides a minimum eruptive age for LVE-P2 as well.

Based on our field and chronological constraints, we infer that LVE-P1 was emplaced before ca. 2,380-2,000 a. Eruptive phase LVE-P2 then occurred at ca. 1,175-550 a, after an approximate hiatus of 800 to 1,800 years (Fig. 5).

## **Other tuff cones**

### *Buhimba and Nyabyunyu tuff cones*

Buhimba and Nyabyunyu are two coalesced tuff cones in the Bulengo area (Figs. 1c, 8a). Different names for these cones have been used in the past, which has led to confusion with the Nyarutshiru tuff cone which lies to the East (Thonnard et al. 1965, Denaeyer 1975). A steep escarpment in the lake-side flank of Buhimba delineates an ancient landslide. A secondary but unclear crater may exist at Nyabyunyu (Fig. 8a). Nyarutshiru and Buhimba mainly consist of consolidated Facies 2 tuffs and lapilli tuffs (Fig. 2d), while the exposed uppermost deposits of Nyabyunyu are alternating Facies 3a coarse and fine tuff with some highly vesicular Facies 3b scoria beds (see Supplementary Materials).

Several open fractures affect the southern flank of Nyarutshiru and the southeastern part of Buhimba. Aligned with these fractures a NNE-SSW oriented fissure produced a small-volume spatter cone and adjacent pahoehoe lava flow at the foot of Buhimba, and partially vegetated scoriaceous spatter levees in the crater of Buhimba (Fig. 8b). This effusive event therefore post-dates the eruptions that constructed Nyarutshiru and Buhimba.

Two paleosol samples taken in the tuff immediately underneath the lava flow which invaded the open craters of Nyabyunyu yielded discordant ages of  $761 \pm 42$  and  $1,365 \pm 34$  a cal. BP (13NYAB0501 and 13NYAB0401; Table 1, Fig. 5, 8c). The minimum eruptive age of Nyabyunyu and the post-Nyabyunyu lava flows is therefore ca. 1,400-700 a.

### *Kirunga tuff cone and Kinungu lava cone*

Kirunga is a tuff cone to the SW of Buhimba-Nyabyunyu (Fig. 1c). Only the uppermost part of its deposits is exposed, displaying bedded Facies 3a coarse and fine tuff (Figs. 8d-e). To its immediate NW lies Kinungu, called Kirunga II by Denaeyer (1975). Kinungu is a cone of Facies 4 welded spatter, similar to that shown in Figure 2l. A NE-SW oriented eruptive fissure runs from the southwestern foot of Kinungu towards the small-volume Kinyogoti tuff cones (Fig. 8d), where it is associated with scoriaceous spatter levees and conelets overlapping the tuff cones. It is however not clear whether the fissure is related to the Kinungu eruption, or postdates it. A lava flow poured out from Kinungu to the NNW into the Bulengo area (Fig. 8d). Two paleosol samples collected in the tuffs near the northwestern base of Kirunga, below the Kinungu lava flow (Fig. 8d-e), yielded radiocarbon ages of  $395\pm51$  and  $117\pm77$  a cal. BP (13KIR0701 and 13KIR0801; Table 1, Fig. 5). More lithofacies details can be found in the Supplementary Materials.

Other small eruptive centers along Lake Kivu's northern shoreline were identified as 'hyaloclastite cones' by Denaeyer (1975) and sampled by Capaccioni et al. (2003). We confirm the nature of the following eruptive centers in the field (Fig. 1c; Supplementary Materials): Facies 2 tuffs and lapilli tuffs at the Bulengo cone and the Kabutembo tuff ring; Facies 3a coarse and fine tuffs at the penultimate phase of Kashaka; Facies 3b ash-and-lapilli tuffs at Nzulu and Kabazana tuff cones, within the Nyamulagira lava flow field (Fig. 2i); Facies 4 magmatic lapilli and scoria at Ndosho and Nengo cones and the uppermost unit of Kashaka (Fig. 2k-l).

Descriptions of hyaloclastite deposits by Denaeyer (1975) resemble our Facies 2 palagonitized tuffs and lapilli tuffs at seven eruptive centers to which access was restricted in 2013 (Fig. 1c): the Kituharu, Kabazana and two Kinyogoti tuff cones, Tshegera in Lake Kivu, the Bushibu tuff ring and the lowermost phase of Kashaka. This results in a total of 24

individual phreatomagmatic vents identified at 15 small eruptive centers along the shoreline of Lake Kivu.

## DISCUSSION

### Eruption mechanisms

Contrasting eruption mechanisms formed the observed phreatomagmatic and magmatic facies (Table 2 and Fig. 2):

**Facies 1 polymict tuff breccias** consist partially of poorly sorted non-vesicular and subangular volcanic clasts with abundant microcrystals, and partially of vesicular vitric fine to coarse ash. We infer the former are accidental lithics from violently excavated bedrock, while the latter are juvenile clasts (Fig. 2f). This facies was therefore generated by explosive blasting through the bedrock during the vent opening phase of the eruption, while the ascending magma reacted with the aquifer in the volcanic rocks close to Lake Kivu.

**Facies 2 tuffs and lapilli tuffs** contain ash aggregates, armored lapilli, impact sags below ballistic blocks and have a high consolidation grade, all of which suggest the presence of liquid water in the eruption column and deposits. The initial magma may have contained enough magmatic volatiles to drive fragmentation and create vesicular pyroclasts. However, the influx of external water into the system likely enhanced fragmentation into abundant fine ash and leading to near-source fallout of ash particles due to wet aggregation. (Koyaguchi and Woods 1996). The large-scale cross-laminations, pinch-and-swell and dune-bedded structures are similar to those described by Brand and Clarke (2012) at the Table Rock Complex, Oregon, USA, and are consistent with the occurrence of erosive high-energy PDC events, thought to have formed at vents below or at lake level. The input of water into the vent needs to be sufficiently high and the magma ascent rate sufficiently low, or the temperature of the propagating dilute PDC needs to decrease enough relative to the temperature at the vent, in

order to generate the typical depositional characteristics (Fisher and Schmincke 1984, Branney and Kokelaar 2002).

**Facies 3 semi-consolidated clast-supported tuff and lapilli tuff** dominantly comprise juvenile coarse ash and small lapilli. The small amount of fine ash (<1%) in Facies 3a and sagged beds below sporadic dm-scale lava lithic blocks and vesicular scoria bombs are suggestive of magma-water interaction and the presence of external water, which is however less pronounced than in Facies 2 deposits. The magma-water interaction for Facies 3a is nevertheless inferred to have been more efficient than during emplacement of near-magmatic Facies 3b, during which were formed scoriaceous fine lapilli beds and a dominance of coarse ash beds, perforated rather than sagged by highly vesicular bombs. Cross laminations, syn-eruptive erosion channels and chute-and-pool structures occur at a smaller scale than in Facies 2. Brand et al. (2014) have shown that lower amounts of liquid water in the eruption column could lead to PDCs with a lower bulk density and thus shorter run-out distances. Additionally, the syndepositional displacements of some portions of LVE-P2 are consistent with a humid nature of the freshly deposited Facies 3 tephra, which failed by gravitational slip on the steep underlying LVE-P1 slopes.

**Facies 4 dry magmatic deposits** were sourced from fissures observed at Buhimba and Kinungu (Fig. 8). As these lava flows and spatter levees cover the phreatomagmatic tuffs, the former must have erupted more recently than the cone-forming eruptions.

The lithofacies sequence at Mt Goma indicates an overall evolution from an explosive and water-rich eruption stage into water-poor or even dry eruption stages. The initial phreatomagmatic vents likely became sheltered from Lake Kivu's surface water by the growing tuff cone, similar to e.g. Surtsey (White and Houghton 2000). At Lac Vert, the proximity of Lake Kivu water, possibly in an aquifer, played a dominant role in the first eruptive phase, while it only contributed water to a limited extent to the active vent of the

second phase 800 – 1,800 years later. Such interactions with the aquifer or surface water and other eruption factors are difficult to constrain however, as illustrated e.g. in the complex sequence of magmatic and phreatomagmatic facies at Mt Gambier, Newer Volcanic Province, Australia (van Otterloo et al. 2013).

### **Chronology of lake level fluctuations and phreatomagmatic eruptions**

The chronology of Lake Kivu water level variations was recently reconstructed from morphological analysis of current lake bathymetry combined with sedimentation rate estimates, radiocarbon dating and bio-chemical proxies in lake sediment cores. These suggest that the level of Lake Kivu was 380 m below its current level at ~12.2 ka and rose to 100 m above the current level in a few thousand (Ross et al. 2014, Zhang et al. 2014) to as little as 200 years (Wood & Scholz 2016). The rapid lake level rise is attributed to either 1.) damming of the outflow of Lake Kivu to the North by VVP volcanism, subsequently forcing its drainage by the Ruzizi river to the South from ~9.7 ka (Ross et al. 2014, Zhang et al. 2014); or 2.) wetter climate conditions, which affected all neighboring East-African rift lakes and resulted in a more rapid response time of the lake level than could be expected from the relatively slow build-up of the lava flow delta from VVP volcanism (Wood & Scholz 2016). During the Holocene, the water level of Lake Kivu then dropped gradually to its current level. The +100 m lake level high-stand must post-date the 11,972±221 a cal. BP eruption that constructed the dry magmatic Nengo scoria cone which lies at the elevation of the current lake level of ~1463 m a.s.l. (Lk-89-02; Table 1; Fig. 1c; Tuttle et al. 1990).

Higher Lake Kivu stands must have shifted the northern shoreline northward in the Holocene, towards Nyamulagira and Nyiragongo, and established shallow lake water or shallow aquifers at the existing eruptive centers. The occurrence of explosive magma-water interaction is thus

in the first order controlled by the availability of external water controlled by Lake Kivu level fluctuations.

In addition to lake level fluctuations, the varying explosivity and efficiency of the magma-water interaction may have been partly controlled by varying magma ascent rates and magma volatile contents between contrasting eruption phases (e.g. Németh et al. 2012; Valentine et al. 2013). Geochemical composition of the magma on the other hand does not seem to have affected the eruption styles, because little differences were found between the different eruptive centers (Cappacioni et al. 2003, Chakrabarti et al. 2009, Barette et al. 2016). Such combination of eruptive and environmental controls could explain the spatial concurrence of dry magmatic and phreatomagmatic centers in the proximity of abundant (aquifer-confined) water of Lake Kivu in the Lac Vert - Bulengo area.

Overall, the occurrence of phreatomagmatism only within ~4 km from the current Lake Kivu's shoreline strongly suggests the process was mainly controlled by the presence or proximity of paleo-Lake Kivu. We thus suggest that all of the identified phreatomagmatic vents must have become active after the lake level rise since ~12.2 ka, with some of them forming in shallow water conditions when the level of Lake Kivu was higher than the current level. Our radiocarbon dates are consistent with such Holocene eruptive ages.

The generally poorly developed paleosols on top of the phreatomagmatic deposits suggest a maximum timespan of 200-500 years between the eruptive phases and subsequent covering by lava flows, taking into account the rapidity of paleosol formation in a tropical climate (James et al. 2000). We infer that the three phreatomagmatic phases of Mt Goma succeeded one another within the same eruptive episode or a few hundred years at maximum, considering they are separated from each other by sharp contrasts in consolidation and facies type, but without evidence of paleosol development. At Lac Vert, a gastropod shell yielded a calibrated age ca. 800-1,000 a younger than the well-developed paleosol in the top of LVE-P1



in which it was found (Table 1; Figs. 5, 7). This represents a time gap between on one hand the end of the LVE-P1 eruption and onset of paleosol formation, and on the other hand the death of the gastropod and burial of its shell within the paleosol. In such manner, the age of LVE-P2 is constrained between the gastropod age and the age of the overlying lava flows, ca. 800-1,800 years after LVE-P1 (Table 1; Fig. 5). At Nyabyunyu, the discrepancy between radiocarbon dates of the same paleosol developed onto the phreatomagmatic deposits (Fig. 5) could be due to 1) an age difference between the smaller and larger crater, i.e. two separate phreatomagmatic events, or 2) the invasion of two separate lava flows 500-600 years apart. Furthermore, several sources of uncertainty may affect the obtained radiocarbon dates, such as the mixed-age nature of paleosols versus single charcoal fragments or shell material, contamination by more recent organic material or an ‘aging’ influence of local volcanic CO<sub>2</sub> degassing (Calderoni and Turi 1998). Despite these potential complications, most of our radiocarbon dates are broadly consistent with each other and with their stratigraphic positions (Fig. 5).

Our radiocarbon dates suggest the occurrence of at least five phreatomagmatic eruptions within the last 2.5 kyr, accounting for an average recurrence rate of ~500 years (Fig. 5; Mt Goma, Lac Vert P1, Lac Vert P2, Kirunga and Nyabyunyu). Additionally, we identify five lava flow events (Fig. 5). Four pre-historical lava flows, most likely sourced from the southwestern fissure zone of Nyiragongo, were emplaced in the Bulengo area within the last ~1.5 kyr. This finding is of specific interest because no lava flows from Nyiragongo have impacted that area during the past ~150 years.

Finally, we also constrain an eruptive age of ca. 1.0-0.8 ka for the Buyinga lava flow, sourced from the N-S-oriented fissure zone extending from the main crater of Nyiragongo to the northern flanks of Mt Goma and Lake Kivu (Thonnard et al. 1965). This immediately constrains a minimum eruptive age of the Mt Goma eruptions. At least one of both events

coincided temporally with the formation of the 765 a cal. BP unusually organic-rich layer encountered in lake sediment cores. Ross et al. (2015) suggest that this layer is the result of a lake mixing event induced by a volcanic eruption which occurred on the lake shore or on the lake floor and disrupted the lake water stratification. At present we do not have sufficient evidence to suggest a causal link between the Mt Goma eruption(s) and the lake mixing event, but our findings provide further insight into potential triggers for lake stratification destabilization. Considering the high population density close to the lake, the chronology of subaerial and sublacustrine eruptions deserves further scientific attention, as do the potential links between subaerial and sublacustrine volcanism and limnic eruptions in the Lake Kivu area.

#### **Spatial pattern of magma-water interaction**

Figure 9 shows a compilation of the 24 phreatomagmatic vents that were identified at 15 phreatomagmatic eruptive centers. This number of phreatomagmatic vents is similar to the amount of individual tephra layers identified in lake sediment cores spanning the last ~10 kyr, and broadly confirm a recurrence of phreatomagmatic eruptions every ~500 years in the area (Wood & Scholz 2016). All the vents can be found within a ~4 km distance from the present shoreline of Lake Kivu, twice as far as previously recognized by Denaeyer (1975) and Capaccioni et al. (2003). Additionally, the NE-SW and N-S fissure networks of Nyiragongo volcano indicate two areas of relatively high eruptive susceptibility between Nyiragongo and the northern part of Lake Kivu (Capaccioni et al. 2003, Chakrabarti et al. 2009).

Magma is able to either ascend vertically directly below the shoreline or migrate laterally through the fissure networks away from Nyiragongo towards the lake shore. We identified an undated small-volume lava flow from a fissure which opened in the Buhimba cone a few tens of m from the present Lake Kivu shoreline (Fig. 8a-b). The NE-SW orientation of this fissure

is consistent with that of the southwestern Nyiragongo fissure network (Smets et al. 2016). During the 2002 Nyiragongo eruption, a series of eruptive fissures opened on the southern flank and a shallow intrusion propagated southwards to Goma. One of the two lava flow branches reached the shoreline without interacting violently with the lake waters (Lorke et al. 2004). Ground deformation data nevertheless suggested a dissociated second deeper intrusion which extended southward beneath the floor of Lake Kivu (Wauthier et al. 2012). Additionally, several tuff rings and maars lie on the lake floor, up to a few km South of the lake's northern shoreline, at a depth of 200-300 m below the current water level, and were formed as the result of subaerial or shallow lacustrine eruptions that occurred during lake level lowstands, i.e. before ~12.2 ka (Ross et al. 2014; Fig. 9). The spatial distribution of these subaqueous vents shows similar alignments than those observed in the Bulengo area. We infer that a 2002-like shallow magmatic intrusion close to Lake Kivu could either result in a dry magmatic eruption or explosive magma-water interaction, while a 2002-like deep intrusion event has the potential to open a vent below the lake floor, with an unknown effect on the lake stratification and the subaerial environment (e.g. Mastin and Witter 2000). No such volcanic event has been experienced in the past 150 years in the Sake-Goma-Gisenyi urban area.

#### **Dilute PDC hazard implications**

Facies 2 and Facies 3 deposits of Mt Goma and Lac Vert indicate that dilute PDC events of varying intensities have occurred in the past. While the impact of tephra fall-out from these relatively small-volume phreatomagmatic eruptions is mostly limited to static loading by wet ash and potential failure of buildings and infrastructure, the lateral impact of ground-hugging and rapidly-moving PDCs represents another severe hazard (e.g. Wilson et al. 2014). We did not observe the full extent of the phreatomagmatic deposits since they are covered by more recent lava flows. The depositional facies of the dilute PDC deposits and the overall

magma compositions of the Virunga rocks (Barette et al. 2016) are nevertheless broadly similar to those of well-studied surge deposits of the Auckland Volcanic Field (AVF), New Zealand (e.g. Brand et al. 2014, Agustin-Flores et al. 2015). Allen et al (1996) suggest that AVF cohesive PDCs did not travel further than 1 - 3 km, while dilute PDCs traveled up to 5 km away from the vent. Taking into account these distances, Figure 9 presents a buffer map of zones potentially impacted in the Holocene by dilute PDCs and limited ash fallout around the phreatomagmatic vents. The map in Figure 9 is a qualitative estimation of the total area potentially impacted by phreatomagmatic ash deposits in the past, and should hence not be interpreted as a probabilistic hazard map. Spatial extent of the deposits depends on the vent location, eruption intensity and duration, and wind direction which varies dominantly between NW and SSW in the area (Dingwell et al. 2016). These parameters will also control the emplacement of future deposits.

About half of the present-day Goma-Gisenyi urban area lies within the 3 km impact zone and almost the entire urban area (>1.2 million inhabitants in 2015) lies within the 5 km impact zone (Fig. 9). This VVP case study demonstrates how relatively small volumes of erupting magma interacting with external water can cause explosive events with potentially severe consequences in a region that is otherwise largely dominated by effusive volcanism. If a phreatomagmatic eruption were to occur in the near future close to the Kivu shoreline, the physical and socio-economic impact could be severe, especially considering the high vulnerability of the conflict-torn population of the East-DRC and border region of Rwanda (Michellier et al. 2016).

## CONCLUSIONS

We provide a stratigraphic description and the first comprehensive Holocene radiocarbon chronology of the phreatomagmatic deposits along the northern shoreline of Lake Kivu:

1. Phreatomagmatic deposits from satellite eruptive centers of Nyiragongo and Nyamulagira volcanoes, along the Lake Kivu shoreline, can be subdivided into three types: Facies 1 polygenetic tuff breccias from vent-clearing explosions, Facies 2 palagonitized tuffs and lapilli tuffs from water-rich phreatomagmatic eruptions and Facies 3 coarse and fine lapilli tuffs from medium-wet to near-dry phreatomagmatic eruptions.
2. At least 24 phreatomagmatic events constructed at least 15 phreatomagmatic tuff cones, rings and maars in the last ~12.2 k.y. within 4 km distance of the current northern shoreline of Lake Kivu. Deposit characteristics suggest that dilute PDC events and ash fallout repeatedly affected most of the presently urbanized area (>1.2 million inhabitants in 2015).
3. New radiocarbon dates indicate the occurrence within the past 2,500 years of at least five lava flow events, two of which occurred in the past 500 years, and at least five phreatomagmatic eruptions with centennial to millennial recurrence rates.
4. The Buyinga lava flow from Nyiragongo occurred 1,000-800 years ago and was preceded, by tens to a few hundred years, by the most recent phreatomagmatic phase of the Mt Goma cone complex. This age is contemporaneous with that of a lake stratification destabilization event in Lake Kivu identified by Ross et al. (2015).
5. A temporal hiatus of 800–1,800 years between the two eruptive phases of the Lac Vert maar volcano suggests that eruptions in “monogenetic” volcanic fields may in fact re-use previously existing magma ascent paths.

518 Our results encourage consideration of explosive magma-water interaction, or  
519 phreatomagmatism, as a likely eruption scenario in the contingency plan and risk management  
520 in the cities of Saké-Goma (DRC) and Gisenyi (Rwanda). The new chronological framework  
521 and lithofacies analysis of the phreatomagmatic eruptions should be extended, both in  
522 terrestrial and sub-lacustrine environments, to further unravel the range of eruptive  
523 mechanisms. This would lead to an improved spatial and temporal susceptibility model for the  
524 phreatomagmatic hazard along Lake Kivu's northern shoreline.

## ACKNOWLEDGEMENT

This work was funded by the Belgian Science Policy (BELSPO) to the project ‘Geo-risk in Central-Africa’ (GeoRisCA, SD/RI/02A, [georisca.africamuseum.be](http://georisca.africamuseum.be)). S. Poppe is currently a Ph.D. aspirant of the Flemish Research Foundation (FWO-Flanders) and additionally supported by Vocatio. B. Smets is funded by the National Research Fund of Luxembourg (AFR PhD Grant n°3221321), K. Fontijn by Natural Environment Research Council grant NE/L013932/1 (RiftVolc). The Goma Volcano Observatory (GVO) and the Belgian embassies in Kigali (Rwanda) and Kinshasa (DRC) are acknowledged for logistic field support. Gastropod determination was carried out by Dirk Van Damme and Pieter Gurdebeke from Ghent University, Belgium. Radiocarbon dating was carried out by Beta Analytic Lab, Florida, USA. Fabien Albino from the RMCA, Tervuren, provided the TanDEM-X-derived DEM, produced in the ViX project funded by BELSPO. Thorough comments by Karoly Németh, Alexa Van Eaton and associate editor Pierre-Simon Ross helped to considerably improve the manuscript. We further thank John Lockwood for providing field note transcripts, and Brittany Brand, Joan Martí, Audray Delcamp, Jean-Christophe Komorowski, Kelly-Ann Ross and many others for helpful discussions.

## REFERENCES

- Agustin-Flores J, Németh K, Cronin SJ, Lindsay JM, Kereszturi G (2015) Shallow-seated explosions in the construction of the Motukorea tuff ring (Auckland, New Zealand): Evidence from lithic and sedimentary characteristics. *J Volcanol Geotherm Res* 304:272-286
- Albino F, Kervyn F, d’Oreye N, Smets B (2015) High-resolution TanDEM-X DEM: An accurate method to estimate lava flow volumes at Nyamulagira volcano (D.R. Congo). *J Geophys Res: Sol E* 120:4189-4207.

550 Allen SR, Bryner VF, Smith IEM, Balance PF (1996) Facies analysis of pyroclastic deposits  
 551 within basaltic tuff-rings of the Auckland volcanic field, New Zealand. *New Zeal J Geol*  
 552 *Geophys* 39:309-327

553 Barette F, Poppe S, Smets B, Benbakkar M, Kervyn M (in press) Spatial variation of volcanic  
 554 rock geochemistry in the Virunga Volcanic Province: Statistical analysis of an  
 555 integrated database. *J Afr Earth Scie*, in press

556 Brand BD, Clarke AB (2012) An unusually energetic basaltic phreatomagmatic eruption:  
 557 Using deposit characteristics to constrain dilute pyroclastic density current dynamics. *J*  
 558 *Volcanol Geotherm Res* 243-244:81-90

559 Brand BD, Gravley DM, Clarke AB, Lindsay JM, Bloomberg SH, Agustin-Flores J, Németh  
 560 K (2014) A combined field and numerical approach to understanding dilute pyroclastic  
 561 density current dynamics and hazard potential: Auckland Volcanic Field, New Zealand.  
 562 *J Volcanol Geotherm Res* 276:215-232

563 Branney MJ, Kokelaar P (2002) Pyroclastic density currents and the sedimentation of  
 564 ignimbrites. *Mem Geol Soc Lond* 27:143

565 Bronk Ramsey C (2009) Bayesian analysis of radiocarbon dates. *Radiocarbon*, 51: 337-360

566 Capaccioni B, Vaselli O, Santo AP, Yalire MM (2003) Monogenic and polygenic volcanoes  
 567 in the area between the Nyiragongo summit crater and the Lake Kivu shoreline. *Acta*  
 568 *Volcanol* 14:129-136

569 Calderoni G, Turi B (1998) Major constraints on the use of radiocarbon dating for  
 570 tephrochronology. *Quat Int* 47:153–159

571 Chakrabarti R, Basu AR, Santo AP, Tedesco D, Vaselli O (2009) Isotopic and geochemical  
 572 evidence for a heterogeneous mantle plume origin of the Virunga volcanics, East  
 573 African Rift system. *Chem Geol* 259:273-289



574 Crowley TE, Pain T (1970) A monographic revision of the African land snails of the genus  
 575 *Limicolaria* Schumacher (Mollusca-Achatinidae). Annales Musée Royal de l'Afrique  
 576 Centrale Tervuren, Scie Zoolog 177:1-61

577 Denaeyer ME (1975) Le glacis des volcans actifs au Nord du Lac Kivu. Mémoires du  
 578 Museum National d'Histoire Naturelle - Série C - Sciences de la Terre 33:79 pp

579 Dingwell A, Rutgersson A, Claremar B, Arellano S, Yalire MM, Galle B (2016) Seasonal and  
 580 diurnal patterns in the dispersion of SO<sub>2</sub> from Mt. Nyiragongo. Atmosph Environ  
 581 132 :19-29

582 Ebinger CJ (1989) Tectonic development of the western branch of the East African Rift  
 583 System. Geol Soc Am Bull 101:885–903

584 Fisher RV, Schmincke H-U (1984) Pyroclastic Rocks. Berlin, Springer-Verlag 472 pp

585 Houghton BF, Wilson CJN, Smith IEM (1999) Shallow-seated controls on styles of explosive  
 586 basaltic volcanism: A case study from New Zealand. J Volcanol Geotherm Res 91:97-  
 587 120

588 Houghton B, White JDL, Van Eaton AR (2015) Phreatomagmatic and related eruption styles.  
 589 In: Sigurdsson H, Houghton B, McNutt S, Rymer H, Stix J (eds) 2015. The  
 590 encyclopedia of volcanoes – Second Edition. Academic Press, San Diego, CA 571-580

591 James P, Chester D, Duncan A (2000) Volcanic soils: their nature and significance for  
 592 archaeology. In: McGuire WG, Griffiths DR, Hancock PL, Stewart IS (eds) (2000) The  
 593 Archaeology of Geological Catastrophes. Geol Soc London Spec Publ 171:317-338

594 Kokelaar P (1986) Magma-water interactions in subaqueous and emergent basaltic volcanism.  
 595 Bull Volcanol 48:275-289

596 Komorowski J (2003) The January 2002 flank eruption of Nyiragongo volcano (Democratic  
 597 Republic of Congo): Chronology, evidence for a tectonic rift trigger, and impact of lava  
 598 flows on the city of Goma. Acta Vulcanol 14:27–62

599 Koyaguchi T, Woods AW (1996) On the formation of eruption columns following explosive  
 600 mixing of magma and surface-water. *J Geophys Res* 101:5561-5574  
 601 Lorke A, Tietze K, Halbwachs M, Wüest A (2004) Response of Lake Kivu stratification to  
 602 lava inflow and climate warming. *Limnol Oceanogr* 49:778–783  
 603 Manville V, Németh K, Kano K (2009) Source to sink: A review of three decades of progress  
 604 in the understanding of volcanoclastic processes, deposits, and hazards. *Sedim Geol*  
 605 220:136-161  
 606 Mastin LG, Witter JB (2000) The hazards of eruptions through lakes and seawater. *J Volcanol*  
 607 *Geotherm Res* 97:195-214  
 608 Michellier C, Pigeon P, Kervyn F, Wolff E (2016) Contextualizing vulnerability assessment: a  
 609 support to geo-risk management in central Africa. *Nat Hazards*, 82:27-42  
 610 Moore JG, Nakamura K, Alcaraz A (1966) The 1965 eruption of Taal Volcano. *Sci* 151:955-  
 611 960  
 612 Németh K, Cronin SJ, Smith IEM, Flores JA (2012) Amplified hazard of small-volume  
 613 monogenetic eruptions due to environmental controls, Orakei Basin, Auckland Volcanic  
 614 Field, New Zealand. *Bull Volcanol* 74:2121-2137  
 615 Pauly BD, Schiffman P, Zierenberg RA, Clague DA (2011) Environmental and chemical  
 616 controls on palagonitization. *Geochem Geophys Geosyst* 12:Q12017  
 617 Reimer PJ, Bard E, Bayliss A, Beck JW, Blackwell PG, Bronk Ramsey C, Grootes PM,  
 618 Guilderson TP, Haflidason H, Hajdas I, Hattz C, Heaton TJ, Hoffmann DL, Hogg AG,  
 619 Hughen KA, Kaiser KF, Kromer B, Manning SW, Niu M, Reimer RW, Richards DA,  
 620 Scott EM, Southon JR, Staff RA, Turney CSM, van der Plicht J (2013). *IntCal13 and*  
 621 *Marine13 Radiocarbon Age Calibration Curves 0-50,000 Years cal BP*. *Radiocarbon*,  
 622 55:1869-1887

623 Ross KA, Smets B, De Batist M, Hilbe M, Schmid M, Anselmetti FS (2014) Lake-level rise  
 624 in the late Pleistocene and active subaquatic volcanism since the Holocene in Lake  
 625 Kivu, East African Rift. *Geomorphol* 221:274-285

626 Ross KA, Schmid M, Ogorka S, Muvundja FA, Anselmetti FS (2015) The history of  
 627 subaquatic volcanism recorded in the sediments of Lake Kivu, East Africa. *J*  
 628 *Paleolimnol* 54:137-152

629 Schmincke H-U, Fisher RV, Waters A (1973) Antidune and chute and pool structures in the  
 630 base surge deposits of the Laacher See area, Germany. *Sedimentol* 20:553–574

631 Smets B, Kervyn M, d’Oreye N, Kervyn F (2015) Spatio-temporal dynamics of eruptions in a  
 632 youthful extensional setting: Insights from Nyamulagira Volcano (D.R. Congo), in the  
 633 western branch of the East African Rift. *Earth-Sci Rev* 150:305-328

634 Smets B, Delvaux D, Ross KA, Poppe S, Kervyn M, d’Oreye N, Kervyn F (2016) The role of  
 635 inherited crustal structures in the development of rift segments: Insights from the Kivu  
 636 basin, western branch of the East African Rift. *Tectonophys* 683:62-76

637 Tazieff H (1977) An exceptional eruption: Mt Niragongo, Jan. 10<sup>th</sup>, 1977. *Bull Volcanol*  
 638 40:189-200

639 Tuttle ML, Lockwood JP, Evans WC (1990) Natural hazards associated with Lake Kivu and  
 640 adjoining areas of the Birunga Volcanic Field, Rwanda and Zaire, Central Africa – Final  
 641 Report. U.S. Geological Survey, Open File Report 90-691

642 Thonnard RLG, Denaeyer NE, Antun P (1965) Carte volcanologique des Virunga (Afrique  
 643 centrale), Feuille no.1, 1:50,000. Centre National de Volcanologie (Belgium),  
 644 Publication no. 32

645 Valentine GA, Fisher RV (2000) Pyroclastic surges and blasts. In: Sigurdsson H, Houghton  
 646 B, Rymer H, Stix J, McNutt S (eds) 2000. *Encyclopedia of Volcanoes*. Academic Press,  
 647 San Diego, CA 571-580

648 Valentine G, Cortés JA (2013) Time and space variations in magmatic and phreatomagmatic  
649 eruptive processes at Easy Chair (Lunar Crater Volcanic Field, Nevada, USA). *Bull*  
650 *Volcanol* 75:752

651 Van Eaton AR, Herzog M, Wilson CJN, McGregor J (2012) Ascent dynamics of large  
652 phreatomagmatic eruption clouds: The role of microphysics. *J Geophys Res*, 117,  
653 B03203, doi: 10.1029/2011JB008892

654 van Otterloo J, Cas RAF, Sheard MJ (2013) Eruption processes and deposit characteristics at  
655 the monogenetic Mt. Gambier Volcanic Complex, SE Australia: Implications for  
656 alternating magmatic and phreatomagmatic activity. *Bull Volcanol* 75:737

657 Wauthier C, Cayol V, Kervyn F, d'Oreye N (2012) Magma sources involved in the 2002  
658 Nyiragongo eruption, as inferred from an InSAR analysis. *J Geophys Res* 117:B05411

659 White JDL, Houghton B (2000) Surtseyan and related phreatomagmatic eruptions. In:  
660 Sigurdsson H, Houghton B, Rymer H, Stix J, McNutt S (eds) 2000. *Encyclopedia of*  
661 *Volcanoes*. Academic Press, San Diego, CA 495-511

662 White JDL, Houghton BF (2006) Primary volcaniclastic rocks. *Geology*, 34:677-680

663 White JDL, Ross P-S (2011) Maar-diatreme volcanoes: A review. *J Volcanol Geotherm Res*  
664 201:1-29

665 Wilson G, Wilson TM, Deligne NJ, Cole JW (2014) Volcanic hazard impact to critical  
666 infrastructure: A review. *J Volcanol Geotherm Res* 286:148-182

667 Wohletz KH (1986) Explosive magma-water interactions: Thermodynamics, explosion  
668 mechanisms, and field studies. *Bull Volcanol* 48:245-264

669 Wood DA, Scholz CA (2016) Stratigraphic framework and lake level history of Lake Kivu,  
670 East African Rift. *J Afr Earth Scie* in press:1-13

671 Zhang X, Scholz CA, Hecky RE, Wood DA, Zal HJ, Ebinger CJ (2014) Climatic control of  
672 the late Quaternary turbidite sedimentology of Lake Kivu, East Africa: Implications for  
673 deep mixing and geologic hazards. *Geology*, G35818.1

674 Zimanowski B, Büttner R, Lorenz V (1997) Premixing of magma and water in MFCI  
675 experiments. *Bull Volcanol* 58:491-495

TABLE CAPTION

**Table 1** Measured and calibrated radiocarbon ages defined from paleosols and shell material at stratigraphical boundaries in phreatomagmatic small eruptive centers on the northern shoreline of Lake Kivu. Samples were pretreated with HCl to remove carbonates. Dating was done at Beta Analytic, Florida, USA, by Accelerator Mass Spectrometry and the resulting ages were calibrated using the Oxcal v.4.2.3 software (Bronk Ramsey 2009) with the IntCal13 curve of Reimer et al. (2013). Outcrop locations are presented in Figs. 3, 6 and 8, with coordinates provided in Supplementary Table S1

**Table 2** Description of the four lithofacies identified in the phreatomagmatic and magmatic deposits at small eruptive centers proximal to the shoreline of Lake Kivu.

FIGURE CAPTIONS

**Fig. 1 a** Location of the Virunga Volcanic Province (VVP) in the western branch of the East-African Rift; major faults are marked in black, international borders in yellow; **b** Hillshade relief image of the VVP based on the SRTM digital elevation model (DEM) at 30 m resolution ([www.usgs.gov](http://www.usgs.gov)); the active volcanoes and their adjacent lava flow fields of Nyamulagira (red field) and Nyiragongo (yellow field) lie within the rift valley, six dormant VVP volcanoes lie on the rift shoulder (pink field); international borders are marked in yellow, the Saké-Goma-Gisenyi urban area houses >1.2 million people (purple area); **c** SRTM-derived hillshade relief image of the northern shoreline of Lake Kivu and bathymetry of the Lake Kivu floor (from Ross et al. 2014); white boxes mark the positions of Figures 3, 5 and 6

**Fig. 2** Lithofacies identified in the small eruptive centers on the northern shoreline of Lake Kivu. Outcrop coordinates are listed in Supplementary Table S1. Facies 1: **a** chaotic polymict tuff breccia at Lac Vert (LVE02); **b** crudely bedded polymict tuff breccia with a m-sized rounded lithic lava block at Lac Vert (LVE27); Facies 2: **c** large-scale cross-bedding in dilute PDC deposits at Mt Goma, the dashed line indicates a truncated surface (MGO44); **d** consolidated tuff and lapilli tuff at Buhimba (BUH11); **e** thin section (plane polarized light) of armored lapilli and ash aggregates in Mt Goma tuffs (MGO08101); **f** characteristic ochre-colored palagonitized armored lapillus in thin section (MGO08101)

**Fig. 2-continued** Facies 3a: **g** dm-sized lithic block with impact sag in Mt Goma tuff (MGO070); **h** dm-scale channel, indicated by the dashed line, created by a dilute PDC in Lac Vert tuff (LVE15); Facies 3b: **i** moderately consolidated tuff and lapilli tuff at Nzulu – pig for scale (NZU05); **j** scoriaceous beds in Mt Goma tuff and lapilli tuff with a vesicular bomb (MGO072); Facies 4: **k** cone-forming scoria deposits at Ndosho (NDO01); **l** welded spatter with crystalline basement xenoliths at Ndosho (NDO09)

**Fig. 3** Pléiades 2013 image (2 m resolution) laid over a TanDEM-X derived hillshade relief image (Albino et al. 2015) of the Mt Goma tuff cone complex (MGO; location in Fig. 1). Outside the cone base (red dashed line) the phreatomagmatic tuffs are masked by more recent lava flows from Nyiragongo.

**Fig. 4** Lithostratigraphic column of the Mt Goma deposits dividing the stratigraphic sequence into three eruptive phases. Phreatomagmatic phase **MGO-P1** with Facies 2 tuffs originates from the SW on-land crater: **a** Dm-scale beds of ochre ash tuffs in the eroded lake-facing cliff, with light-grey, cm-sized and angular lithic clasts from pre-MGO lava flows - hammer for

scale (MGO44). Phreatomagmatic phase **MGO-P2** Facies 3a tuffs originate from the NE on-  
land crater: **b** Contact between the indurated Facies 2 ash tuffs of MGO-P1 and the Facies 3a  
cm-scale cross-bedded laminae of mildly indurated dark-grey slightly vesicular coarse tuffs of  
MGO-P2 – shovel for scale (MGO56). Phreatomagmatic phase **MGO-P3** produced the most  
voluminous deposits with alternations of Facies 3a and 3b tuffs and the inferred source was in  
the flooded largest crater: **c** Sequence of dm-scale subunits with clast-supported laminae, with  
contrasting median grain size and proportions of fine ash; note the angular lithics from pre-  
MGO lava flows and the scoriaceous coarsest fraction (MGO64); **d** Chute-and-pool structure  
cut by a fine-grained bedded PDC deposit within the parallel bedded cm-scale laminae of  
finer and coarser juvenile ash of MGO-P3; fine ash constitutes < 1% here (MGO18); **e** Top of  
the MGO sequence at its northwestern, most distally exposed side, with paleosol sample  
MGO19020201, covered by more recent lava of the Buyinga flow (Thonnard et al. 1965)

**Fig. 5** Age probability distributions at 95.4% ( $2\sigma$ ) confidence interval for paleosol, charcoal  
and shell samples from selected phreatomagmatic and lava flow deposits along the northern  
shoreline of Lake Kivu (Table 1; sampling locations in Table S1). Samples collected between  
a tuff deposit and a more recent lava flow simultaneously provide a maximum lava flow age  
and a minimum age of the phreatomagmatic event

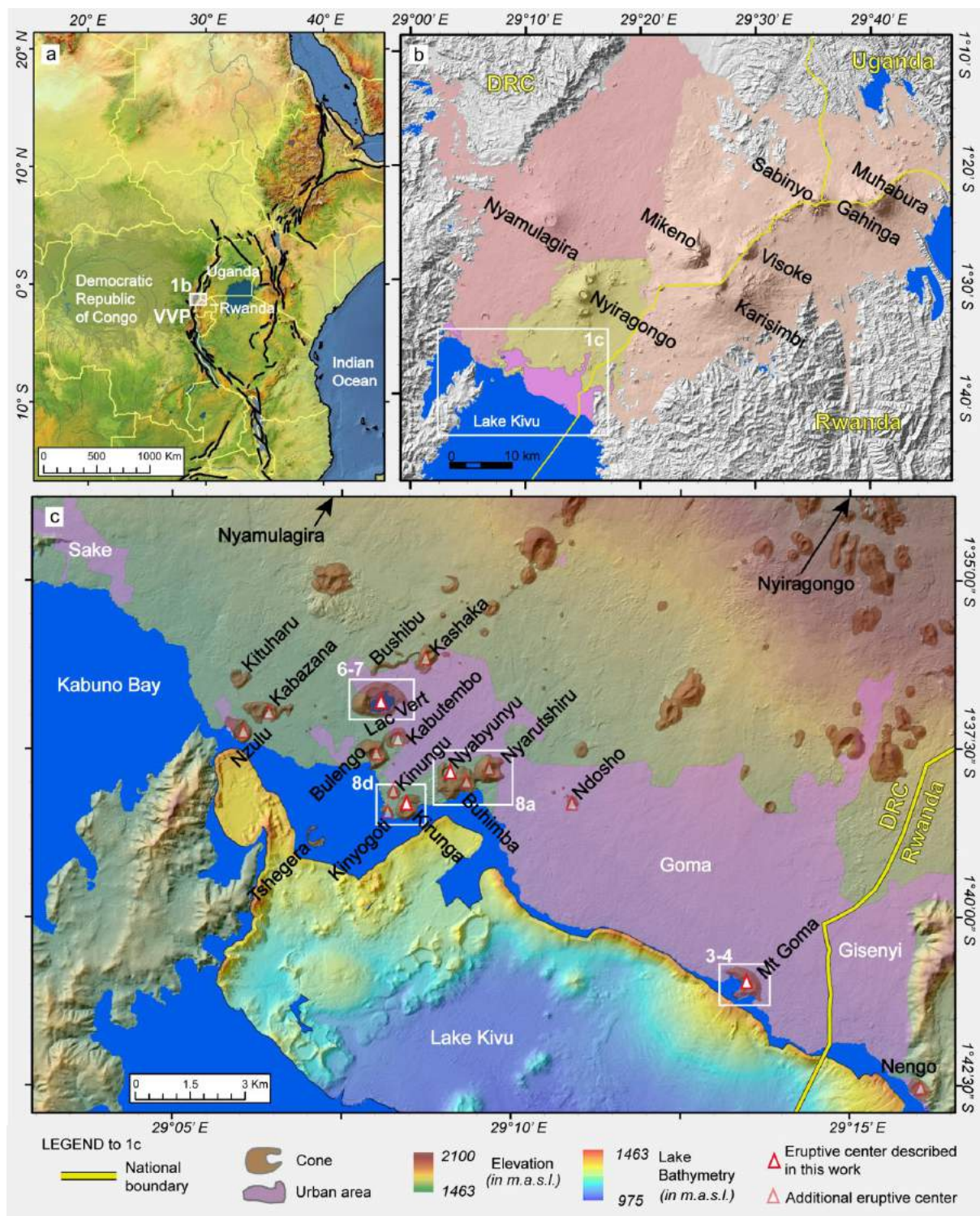
**Fig. 6** Pléiades 2013 image (2 m resolution) laid over a TanDEM-X derived hillshade image  
(Albino et al. 2015) of the Lac Vert maar complex with its surrounding tuff ring (LVE;  
location in Fig.1). Outside the maar ejecta ring base, the tuffs are covered by more recent lava  
flows.



**Fig. 7** Lithostratigraphic column dividing LVE into deposits from three eruption phases observed in the field. The first-phase deposit **LVE-P1** is composed of a lower Facies 1 **LVE-P1-1: a.** Chaotic breccia tuff composed of grey fine ash with polymict mm- to dm-sized angular lithics from pre-LVE lava flows and basement rocks (LVE02, see also Fig. 2a); and an upper phreatomagmatic Facies 2 bedded **LVE-P1-2: b** Dm-scale beds of palagonitized Facies 2 tuff with ~10% cm-sized lithics and >25% vesicular ash-coated lapilli and ash aggregates - hammer for scale (LVE26). The second Facies 3a phreatomagmatic deposit **LVE-P2** is found around the northern crater (see also Fig. 2h): **c** Contact between the weathered top of LVE-P1 and the Facies 3a phreatomagmatic tuff of LVE-P2 with terrestrial gastropod shells, genus *Limicolaria* (LVE240201, Table 1). A third small-volume eruptive phase **LVE-P3** formed an ejecta ring of Facies 1 breccia around a ~20 m wide crater nested within the northern LVE crater; **d** More recent basaltic lava flows cover the LVE-P2 tuffs, the orange-brown boundary between the two is a thin paleosol (LVE12-LVE13; Table 1)

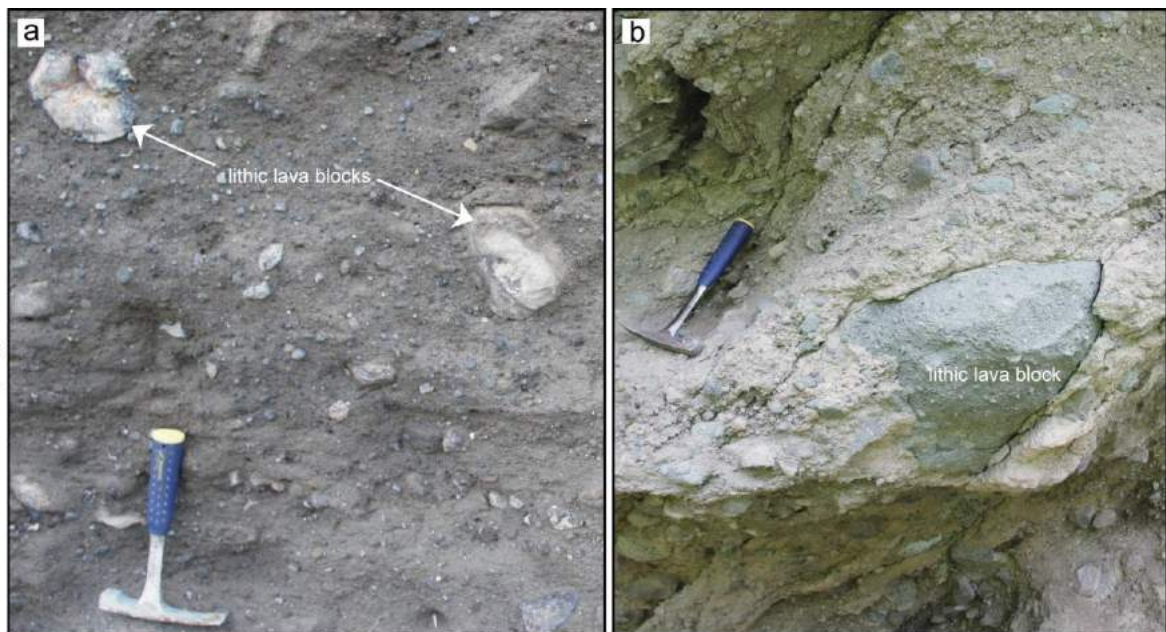
**Fig. 8 a** TanDEM-X derived hillshade relief image (Albino et al. 2015) of the aligned cones Nyarutshiru, Buhimba and Nyabyunyu (location in Fig.1c) with the locations of paleosol samples NYAB04 and NYAB05 (Table 1); **b** Small-volume pahoehoe lava flow from a fissure in the eastern flank of Buhimba, correlated to the spatter levees inside the Buhimba crater (BUH02); **c** Location of paleosol sample NYAB04 at the contact between late-eruptive coarse to fine ash beds of the Nyabyunyu tuff cone and its post-eruptive crater-filling lava flow; **d** Hillshade relief image of the Kirunga tuff cone, smaller Kinyogoti tuff cones with a nested eruptive fissure and associated spatter levees, and the Kinungu spatter cone and lava flow (location in Fig.1c); **e** Contact between the Kirunga coarse to fine tuffs and the Kinungu lava flow, and location of paleosol sample KIR070201

**Fig. 9** Spatial extent of the area potentially impacted in the past by more cohesive (1 km extent) or more dilute (5 km extent) PDCs from past phreatomagmatic eruptive vents in the Sake-Goma-Gisenyi urban area as identified in the field and from the literature (background: TanDEM-X DEM hillshade image from Albino et al. 2015; Lake Kivu bathymetry from Ross et al. 2014). All marked subaerial phreatomagmatic vents (red triangles) are inferred to be of Holocene age, while the currently sublacustrine tuff rings and cones (blue dots) are assumed to have formed during periods of lower lake levels before ~12.2 ka (Ross et al. 2014). Note that when combined, the high-intensity PDC impact zones within 5 km around each identified vent comprises almost the entire currently urbanized area. The impact and spatial extent of PDCs (and ash fall) during a potential future phreatomagmatic eruption in the urban area would depend on the future vent location, eruption intensity and duration, and wind direction. This map presents a qualitative estimation of the total area that may have been impacted in the past by phreatomagmatic deposits from small eruptive centers, and should not be interpreted as a probabilistic hazard map.

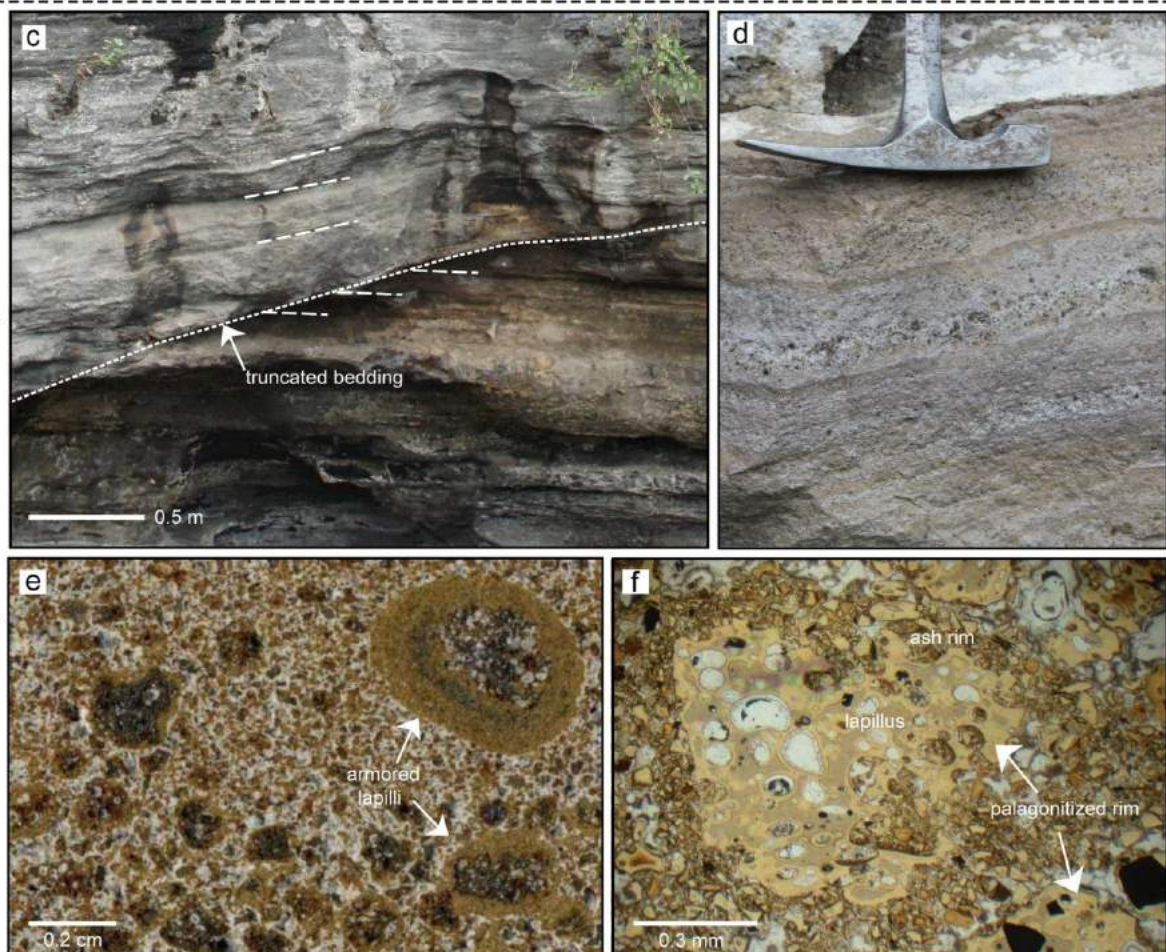




Facies 1 - polymict tuff breccia

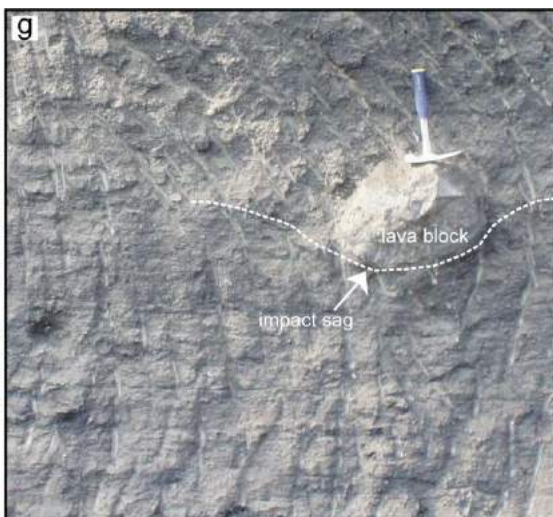


Facies 2 - palagonitized tuff and lapilli tuff





Facies 3a - coarse to fine tuff

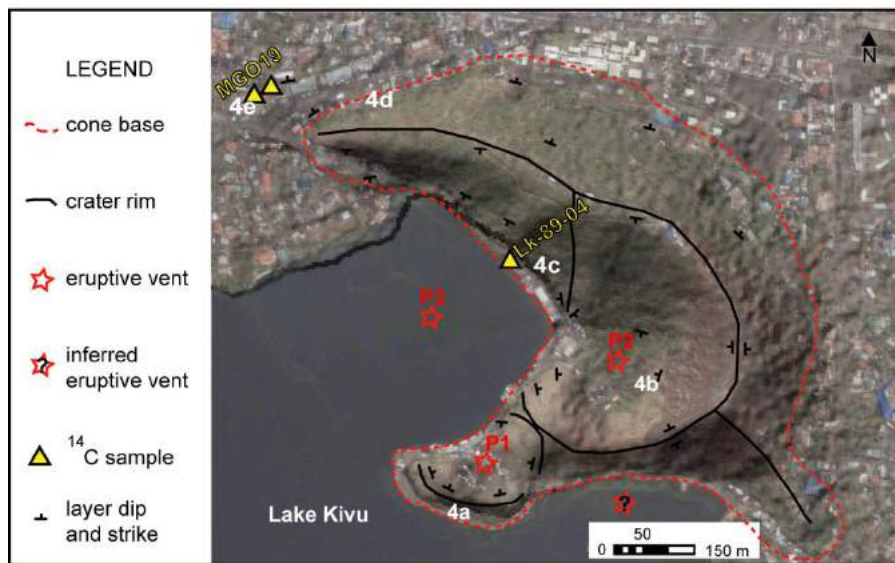


Facies 3b - tuff and lapilli tuff



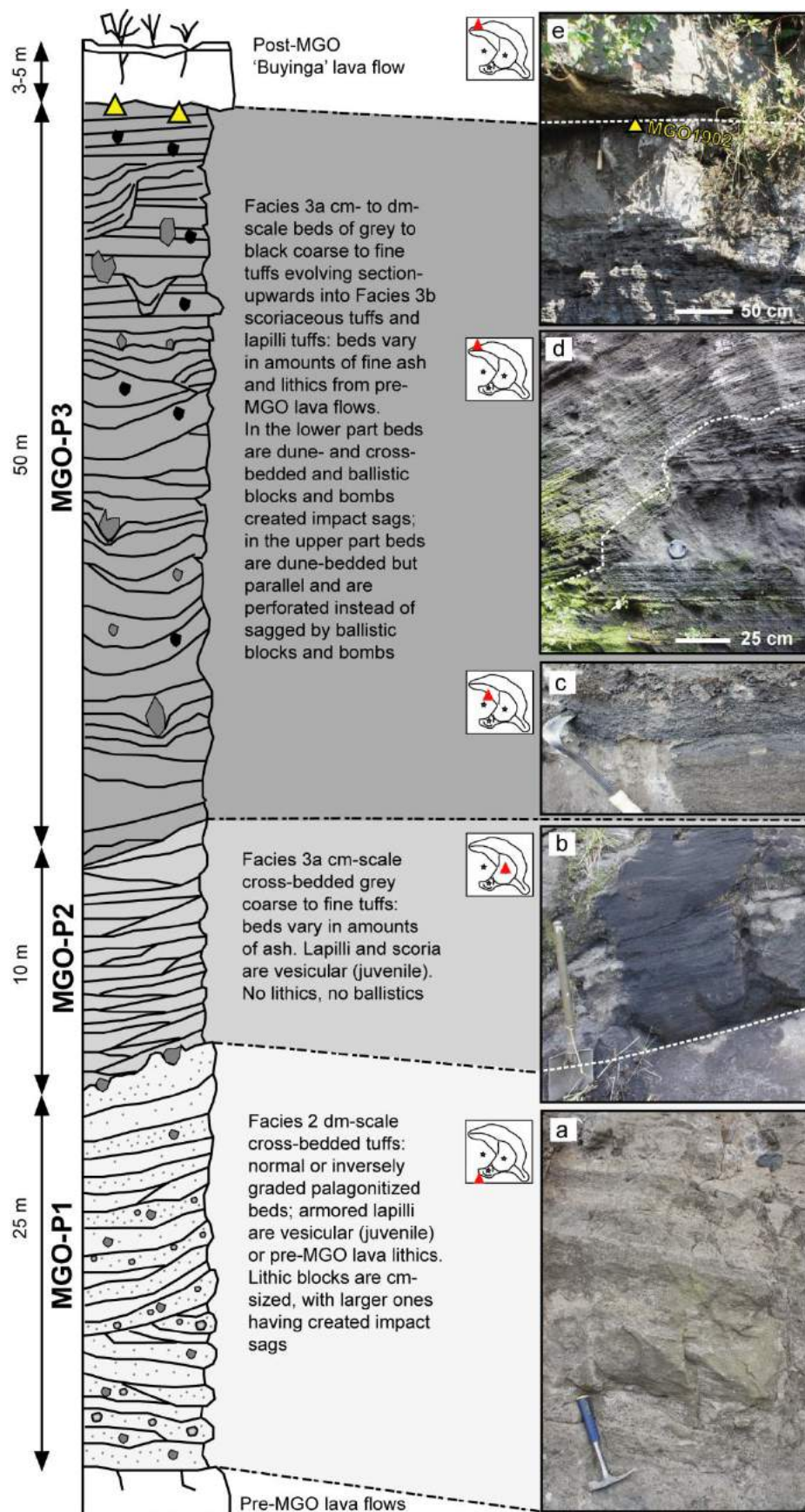
Facies 4 - scoria, spatter, lava

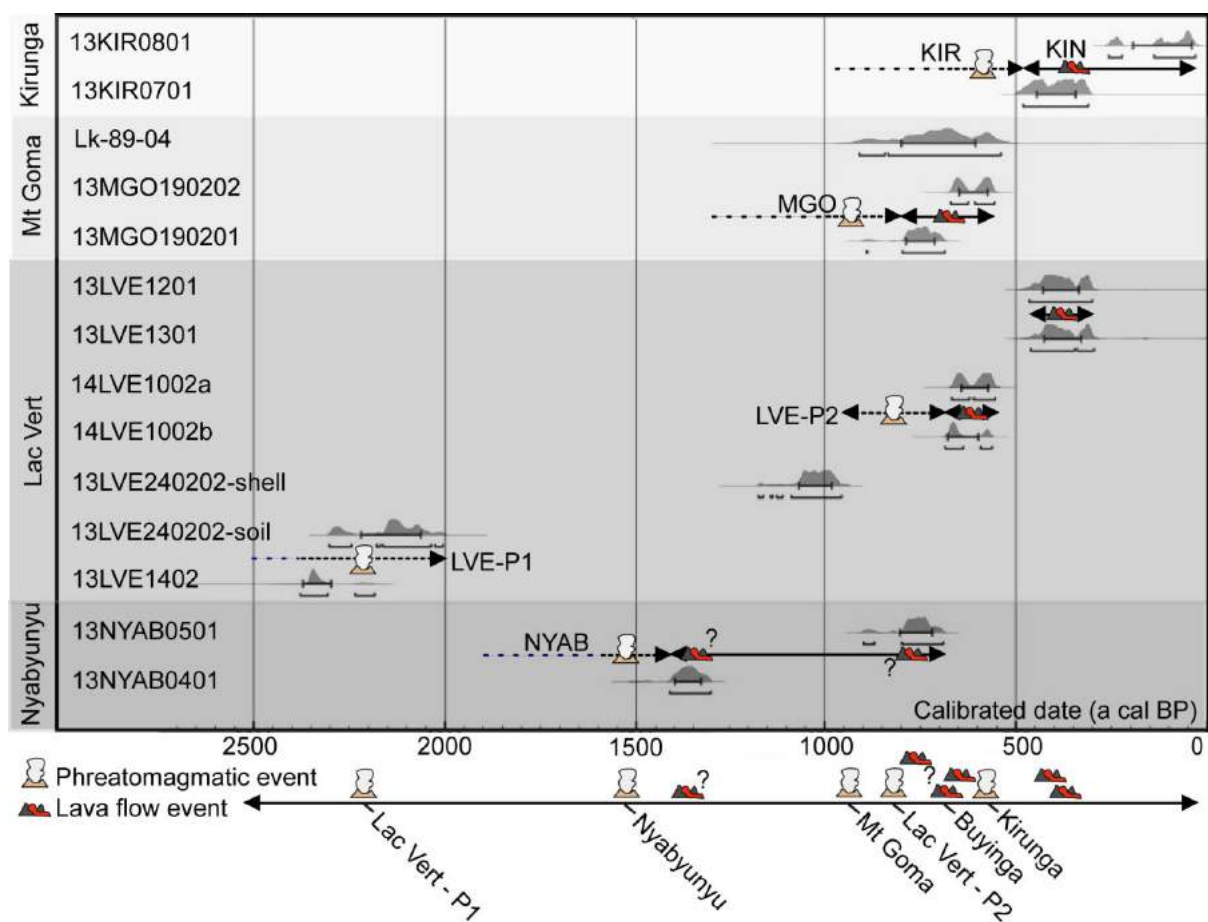




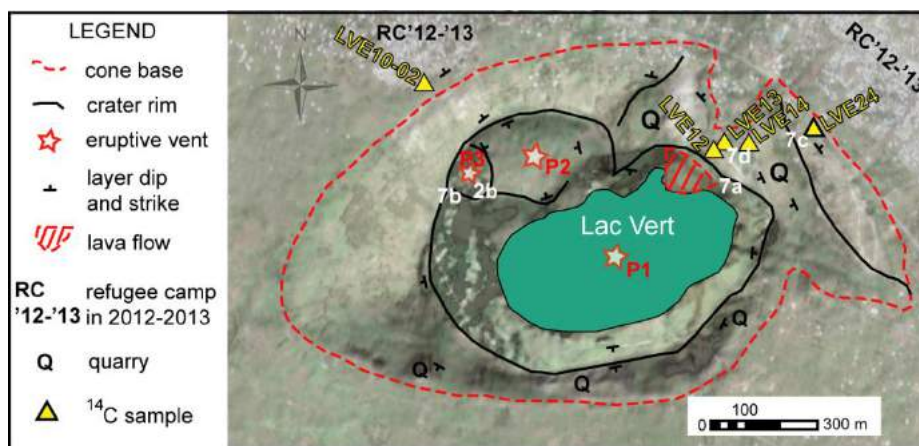
Poppe\_etal\_Fig\_3





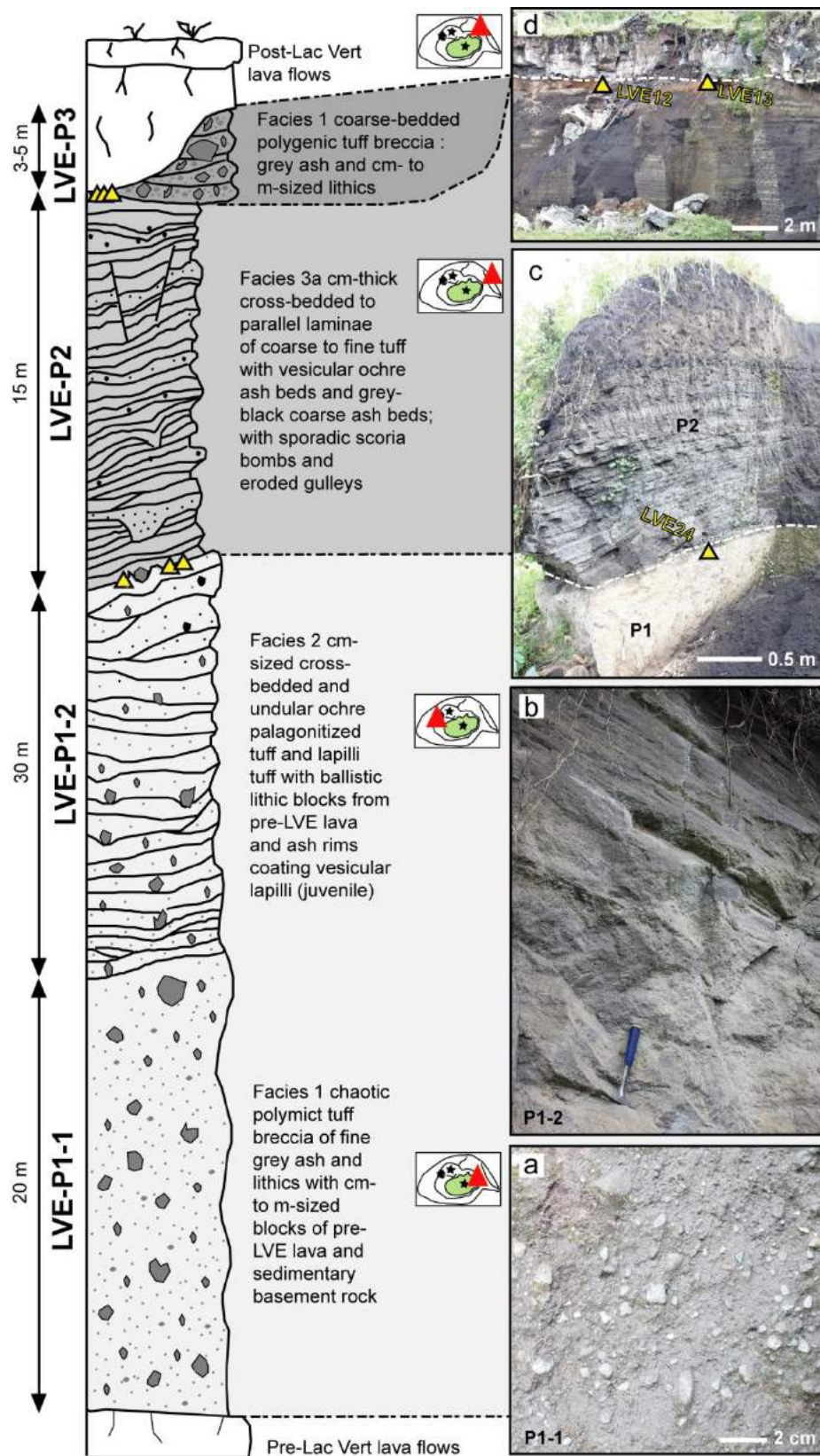


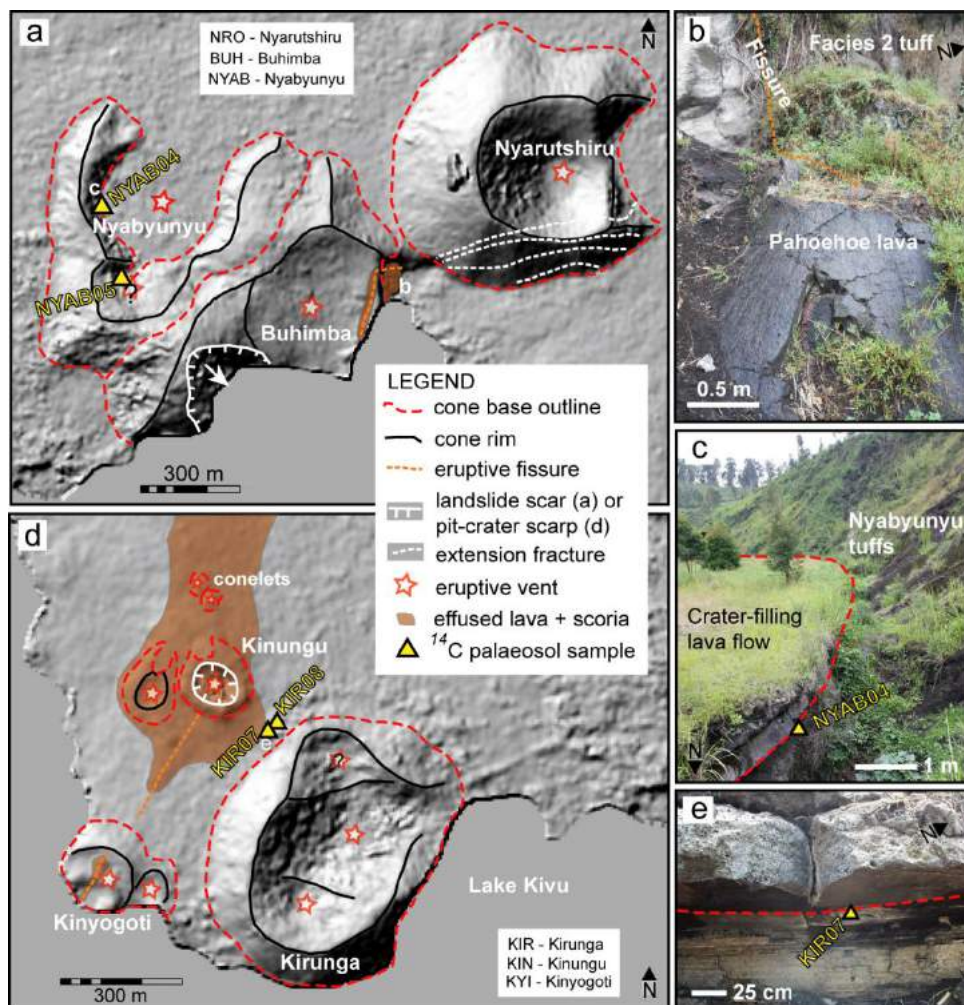
Poppe\_etal\_5



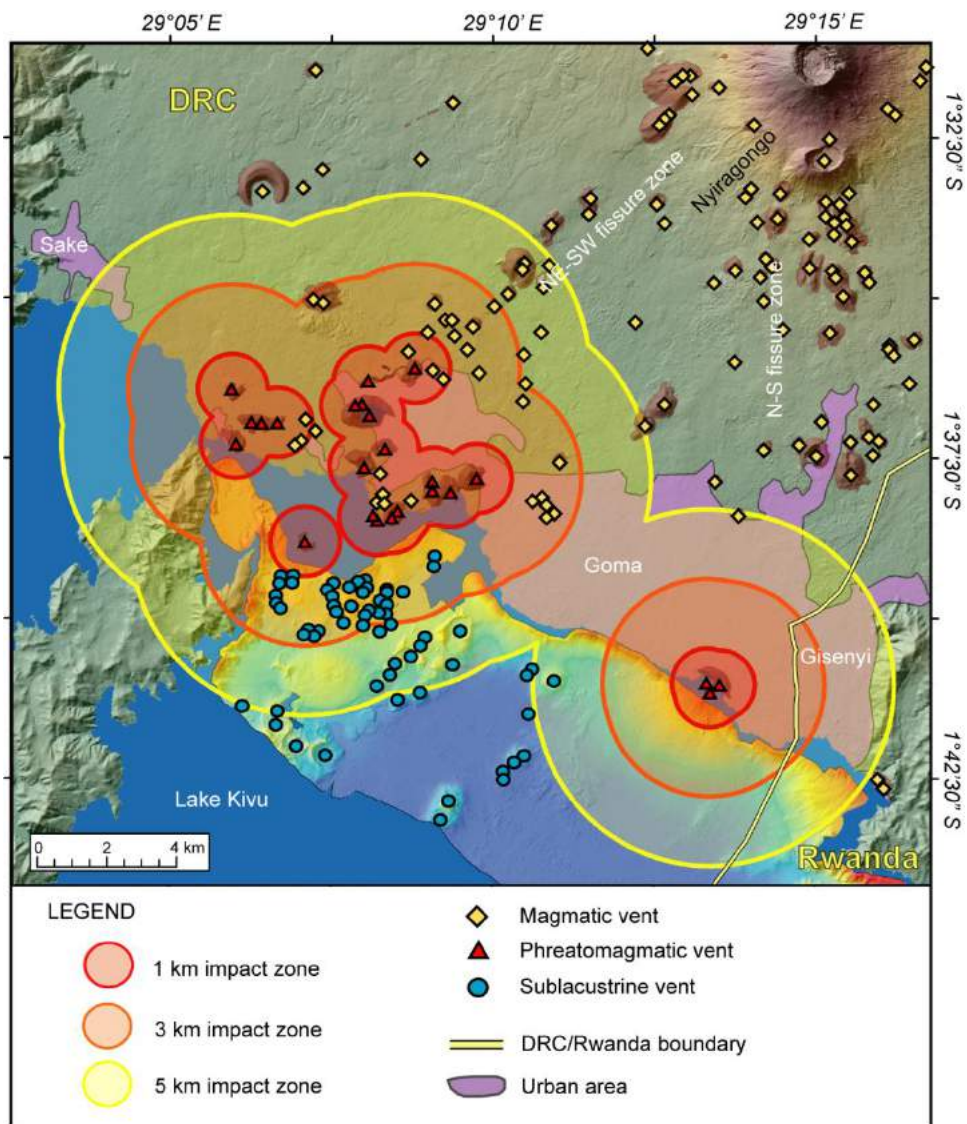
Poppe\_etal\_Fig\_6











Poppe\_etal\_9

808 Table 1

Sample	Beta Analytic Lab Code	Sample type and stratigraphic relation	Measured $^{14}\text{C}$ age (yr BP)	Calibrated Mean age (a cal BP $\pm 1\sigma$ )	Calibrated age range $2\sigma$ (a cal BP)	$^{13}\text{C} / ^{12}\text{C}$ (+/-0.5‰)
13KIR801	371363	Paleosol in top deposits of Kirunga	$60 \pm 30$	$117 \pm 77$	<b>31</b> - 139 (72.3%); 222 - <b>258</b> (23.1%)	-25.9
13KIR0701	371362	Paleosol in top deposits of Kirunga	$340 \pm 30$	$395 \pm 51$	<b>311 - 481</b>	-27.3
Lk-89-04 <sup>a</sup>	N/A	Charcoal in top deposits of Mt Goma – Phase 3	$740 \pm 110$	$703 \pm 97$	<b>539</b> - 834 (86.7%); 842 - <b>910</b> (8.7%)	/
13MGO190202	371354	Paleosol in top deposits of Mt Goma – Phase 3	$650 \pm 30$	$611 \pm 37$	<b>556</b> - 607 (51.9%); 625 - <b>670</b> (43.5%)	-23.5
13MGO190201	371353	Paleosol in top deposits of Mt Goma – Phase 3	$840 \pm 30$	$749 \pm 37$	<b>686</b> - 797 (95.0%); 888 - <b>891</b> (0.4%)	-24.3
13LVE1201	371355	Paleosol in top deposits of Lac Vert – Phase 2	$310 \pm 30$	$382 \pm 47$	<b>301 - 465</b>	-18.9
13LVE1301	371356	Paleosol in top deposits of Lac Vert – Phase 2	$300 \pm 30$	$378 \pm 48$	<b>296</b> - 340 (25.8%); 347 - <b>461</b> (69.6%)	-19.7
14LVE1002 <sup>a</sup>	386922	Paleosol in top deposits of Lac Vert – Phase 2	$640 \pm 30$	$608 \pm 35$	<b>554</b> - 610 (54.4%); 621 - <b>668</b> (41.0%)	-20.0
14LVE1002b	386921	Paleosol in top deposits of Lac Vert – Phase 2	$690 \pm 30$	$638 \pm 40$	<b>562</b> - 593 (26.5%); 638 - <b>685</b> (68.9%)	-22.1
13LVE240202 <sup>a</sup>	371366	Terrestrial gastropod shell in top deposits of Lac Vert – Phase 1	$1,120 \pm 30$	$1,024 \pm 43$	<b>956</b> - 1,088 (91.8%); 1,109 - 1,124 (1.4%); 1,135 - 1,141 (0.5%); 1,160 - <b>1,173</b> (1.7%)	-10.5
13LVE240202b	371367	Paleosol in shell in top deposits of Lac Vert – Phase 1	$2,140 \pm 30$	$2,142 \pm 78$	<b>2,006</b> - 2,026 (3.2%); 2,037 - 2,162 (71.2%); 2,169 - 2,179 (1.5%); 2,244 - <b>2,302</b> (19.5%)	-21.4
13LVE1402	371358	Paleosol in top deposits of Lac Vert – Phase 1	$2,320 \pm 30$	$2,334 \pm 37$	<b>2,184</b> - 2,235 (5.3%); 2,306 - <b>2,378</b> (90.1%)	-17.6
13NYAB0501	371364	Paleosol in top deposits of Nyabyunyu	$850 \pm 30$	$761 \pm 42$	<b>690</b> - 799 (90.2%); 870 - <b>898</b> (5.2%)	-21.5
13NYAB0401	371365	Paleosol in top deposits of Nyabyunyu	$1,480 \pm 30$	$1,365 \pm 34$	<b>1,305 - 1,412</b>	-20.2
Lk-89-02 <sup>a</sup>	N/A	Charcoal below the base of Nengo scoria cone	$10,240 \pm 30$	$11,972 \pm 221$	<b>11,411</b> - 11,429 (0.4%); 11,495 - 11,545 (1.4%); 11,601 - <b>12,411</b> (93.6%)	/

809

810 <sup>a</sup> Measured ages from Tuttle et al., 1990; re-calibrated with Oxcal v4.2 and the Intcal13-curve

811

812 Table 2

813

<b>Facies name</b>	<b>Facies description</b>
<b><i>Facies 1</i></b> Polymict tuff breccia (Fig. 2a, b)	Poorly-sorted; chaotic to crudely bedded; dm- to m-sized blocks are lithics from pre-existing lava flows (low vesicularity, subangular shape, high amounts of different crystal types); (semi-)consolidated grey matrix consists of juvenile fine lapilli and ash (high vesicularity, angular shape, vitric) and lapilli- to ash-sized pulverized lithics
<b><i>Facies 2</i></b> Palagonitized tuff and lapilli tuff (Fig. 2c-f)	Consolidated beds of >50% fine ash, 5-20% mm- to cm-sized lithic clasts and 20-30% of vesicular (juvenile) lapilli; armored lapilli with 0.5-3 cm-sized solid core and 1-5 mm coating of fine ash; ash aggregates; impact sags; m-scale cross-bedding; pinch-and-swell beds; partial palagonitization of vitric ash fraction resulted in ochre-colored deposits
<b><i>Facies 3a</i></b> Coarse to fine tuff (Fig. 2g, h)	Centimetric alternations of poorly consolidated moderately to well-sorted coarse to fine ash with impact sags from dm- to m-sized lithic ballistic blocks of pre-existing lava; small-scale cross-bedding, pinch-and-swell textures between individual beds; dm-deep erosion channels; chute-and-pool structures
<b><i>Facies 3b</i></b> Tuff and lapilli tuff (Fig. 2i, j)	Moderately consolidated and sorted cm-scale alternations of coarse ash and vesicular lapilli; <1% fine ash; higher amount of vesicular juvenile clasts compared to Facies 3a; bed perforations by dm- to m-sized lithic blocks and vesicular volcanic bombs; chute-and-pool structures; dm-deep erosion channels
<b><i>Facies 4</i></b> Scoria, spatter and lava (Fig. 2k, l)	Highly vesicular brown to black welded lava spatter and bombs and angular lapilli; welded spatter from lava fountains; xenoliths from the crystalline basement; spatter levees along eruptive fissures; lava mounds; lava flows

814

815

816